

Thermal description and entropy evaluation of magnetized hybrid nanofluid with variable viscosity via Crank–Nicolson method

Hanifa Hanif^{a,b}, Wasim Jamshed^c, Suriya Uma Devi S^d, Mohamed R. Eid^{e,f,*},
Sharidan Shafie^b, Rabha W. Ibrahim^{g,h,i}, Nor Ain Azeany Mohd Nasir^j,
Assmaa Abd-Elmonem^k, Sayed M. El Din^l

^a Department of Mathematics, Sardar Bahadur Khan Women's University, Quetta, Pakistan

^b Department of Mathematical Sciences, Faculty of Science, Universiti Teknologi Malaysia, 81310, Johor Bahru, Johor, Malaysia

^c Department of Mathematics, Capital University of Science and Technology (CUST), Islamabad, 44000, Pakistan

^d Department of Mathematics, KPR Institute of Engineering and Technology, Coimbatore, 641407, India

^e Department of Mathematics, Faculty of Science, New Valley University, Al-Kharga, Al-Wadi Al-Gadid, 72511, Egypt

^f Department of Mathematics, Faculty of Science, Northern Border University, Arar, 1321, Saudi Arabia

^g Near East University, Mathematics Research Center, Department of Mathematics, Near East Boulevard, PC:99138, Mersin 10, Nicosia, Turkey

^h Department of Computer Science and Mathematics, Lebanese American University, Beirut, Lebanon

ⁱ Information and Communication Technology Research Group, Scientific Research Center, Al-Ayen University, Thi-Qar, Iraq

^j Department of Mathematics, Centre for Defence Foundation Studies, Universiti Pertahanan Nasional Malaysia, Kem Sungai Besi, 57000, Kuala Lumpur, Malaysia

^k Department of Mathematics, College of Science, King Khalid University, Abha, Saudi Arabia

^l Center of Research, Faculty of Engineering, Future University in Egypt New Cairo, 11835, Egypt

ARTICLE INFO

Keywords:

Hybrid nanofluid
Magnetohydrodynamic
Entropy generation
Crank–Nicolson method

ABSTRACT

The dominant characteristics of hybrid nanofluids, such as low cost, improved heat transfer rates, and higher thermal and electrical conductivity, make them preferable fluids in thermal energy systems. In light of these incredible features, our goal in the present research is to analyse heat transfer and entropy generating in (Fe₃O₄–Cu)/water hybrid nano liquid flowing via a vertical cone with variable wall temperature inserted in a porous material. The effects of variable viscosity, magnetic force, and thermal radiative flux are additional aspects that contribute to the originality of the constructed model. The mathematical model is solved utilising the Crank–Nicolson technique, and the numerical findings are showed graphically and in a tabular manner. The heat transfer process is improved by hybrid nanoparticles and porosity while being hindered by magnetic interaction, viscosity, and thermal radiation. Energy loss in the form of increased entropy can be noted at the further vertical end of the cone than the base. The parametrical influence was reported to be nominal compared to the other physical aspects. Domination of heat transfer induced entropy generation and be observed for the porosity improvements.

1. Introduction

The thermal engineering notion of heat transfer (HT) handles energy conversion, exchange, production, and absorbing.

* Corresponding author. Department of Mathematics, Faculty of Science, New Valley University, Al-Kharga, Al-Wadi Al-Gadid, 72511, Egypt.
E-mail address: m_r_eid@yahoo.com (M.R. Eid).

<https://doi.org/10.1016/j.csite.2023.103132>

Received 25 February 2023; Received in revised form 18 May 2023; Accepted 25 May 2023

Available online 30 May 2023

2214-157X/© 2023 The Authors. Published by Elsevier Ltd. This is an open access article under the CC BY-NC-ND license (<http://creativecommons.org/licenses/by-nc-nd/4.0/>).

Convection, transmission, and radioactivity are the three methods used to carry energy. Essentially, the molecules are spread by convection when the temperature is practical. Blood flow in warm-blooded animals, hot air balloons, hot water, and air conditioners are a few examples of convective HT. Numerous scientific simulations were employed by the researchers, including those by Jeffery, Carreau, Maxwell, Cross, Casson, and power law fluid, to conduct their experiments on convective HT. Manzur et al. [1] looked at the impacts of HT, suppleness assistance, and postponing activities after mixed convection. Their research and investigation support the claim that a rise in the Nusselt number increases HT. Hayat et al. [2] considered the Cross-fluid statistical mode paired with the mathematical demonstration of HT of magnetized strained shallow. The most recent effort at HT by shrinking slip current radioactivity, suction, and injection is assessed by Jamaludin et al. [3]. According to Vaisi et al. [4], heat transmission in a multi-fluid compressed via a strip and wavy fins has been studied and performed. Hanifa [5] discussed heat and mass transference in a nano liquid for cooling implementations. Saqib et al. [6] presented HT analysis of Maxwell fluid using the Cattaneo-Fredrich model. Different mathematical analyses of HT were presented by several authors [7–12].

Conservation of energy is now more important than producing energy. Entropy production is one source of energy loss. To find an optimal design, it is necessary to reduce the entropy effect within the design of thermodynamic implementations. Bejan [13] was the first to introduce the notion of entropy-generating minimisation. Later, adopting that approach, other researchers investigated the entropy production in porous confined enclosures with barriers (Datta et al. [14]) and saturation with nanofluid [15–18]. They demonstrated how entropy production influences the thermal efficiency of the issue. In addition, the assessment has been expanded to include an open chamber. Hussain et al. [19] investigated the creation of entropy in a porousness-tilted open channel using a nanofluid. The study's findings showed that the low porosity variable can decrease entropy formation. Al-Rashed et al. [20] used numerical methods to solve the isothermal block put in the nano liquid-covered cubic open enclosed space issue. The findings indicate that increasing the block size leads to a greater Bejan quantity, which is related to entropy. Similarly, numerous research works were attempted to explore the Entropy loss over various shapes [21–24].

Hybridity nanofluids (HNFs) have special properties that make them helpful in a range of HT presentations. When utilised with the wrong fluid, these instruments improved HT functional measurements and their behaviour. Outstanding its extensive engineering and industrial research requirements, the idea of boundary point flowing of HNFs via expandable shallow developed further noticeably years ago. The researchers have given rehabilitation of HNFs that destroy HT much thought because of their amenability to the various uses of HNFs. Hanif and Shafie [25–27] presented several studies on HT and the flowing of HNF via a horizontal surface using the fractional Maxwell model. To increase the rate of HT obtained by broadening the slide even further, Said et al. [28] purported a 3D status of HNFs. Mandal et al. [29] used an artificial neural network to offer analytical measurements. Dubey et al. [20] have briefly examined HNF on technical improvements. The examination [30] studied the migration of a stretchable plate's magneto tangent HNF via the boundary layer. Qureshi [31] and Parvin et al. [32] also tested the expanded HT of tangent hyperbolic fluids across a nonlinear wavey transparency that incorporated HNFs. In a survey on the HT and rheologic estates of HNFs, researchers have made contributions to and documented several investigations in this area [33–37].

The magneto impacts on flowing electrical charge, electrical current, and magneto substances are referred to as a magnetic field (MF), which is a vector field. In MF, a moving charge encounters a force that is perpendicular to both the magnetic field and its speed. Zhang et al. [38] presented a study in HNFs movement near elastic superficial with Ta and Ni nano molecules underneath the inspiration of an encouraged MF. Izadi et al. [39] considered the natural convection of HNFs exaggerated by a motivated periodic MF inside a porous medium. Khan et al. [40] introduced a comparative examination of HT and resistance slog in the movement of several HNFs affected by correlated MF and nonlinearly energy. Mourad et al. [41] reported a computational examination employing the Galerkin finite element assessment of current aspects of HNFs occupied in curly inclusion with uniform MF effect. Talebi et al. [42] investigated the mixture-based dusty HNFs' progress in porousness materials exaggerated by MF utilising RBF procedure. Rashidi et al. [43] gave a computational model of HNFs assorted convective flow in a square hole with MF utilising a high-order compact arrangement. Biswas et al. [44] suggested a narrative loom of HNFs curly enclosed tilted porous enclosure striking a partially active MF.

An oblique plane with a free surface is explored to see how a fluid flow with a temperature-dependent variable viscosity affects (VVA) movement. Since there is little fluid film, a rough estimate of lubrication can be used. The fluid viscosity decreases exponentially with temperature and is affected by convective heating effects. This concept is suggested by much research in HNFs. For example, Aanam et al. [45] used VVE in a rotation modulation on Ferro convection. Idowu et al. [46] utilised HT movement of dissipative Casson fluid with VVF and current conductivity possessions. Akbar and Abbasi [47] measured VVE on the peristaltic signal with entropy generation. Jan et al. [48] recommended a computation of the attracted Couette–Poiseuille current movement of couple pressure among two parallel sheets with VVE. Ismail et al. [49] utilised the concept of fractional calculus of thin-film movement in the attendance of thermal conductance and VVE.

The term “thermal radiation” (TR) refers to electromagnetic radiation that is produced by matter as a result of its heat and whose physiognomies vary on the matter's temperature. The infrared radiation emitted by an electric heater or traditional internal radiator is an illustration of TR. Xu et al. [50] presented an analysis work on HS, TR, and heat transport of NFs in porousness materials. Wakif et al. [51] probed the thermal magnetohydrodynamic constancy of Al_2O_3 –CuO HNFs by analysing the TR properties. Chen et al. [52] researched the effects of NFs combination on NFs' TR holdings. Agrawal et al. [53] administered the movement of HNFs with TR and HS influences via a large area of porous material that appeared to be deeply embedded. Prakash et al. [54] used peristaltic motion to pump magneto NFs with TR and features of heat-reliant on viscid. Utilising a finite element technique, Khan et al. [55] produced a magneto dipole and TR effects on the stagnating point flow of micropolar-based NFs via a rapidly extendable slippage. A comparison analysis of quivering magneto Falkner–Skan wedge flowing for non-Newtonianism NFs was presented by Ali et al. [56], considering TR and motivating energy. Shaw et al. [57] studied magneto flowing of fractious HNFs driven by linearly, nonlinearly, and quadratic TR

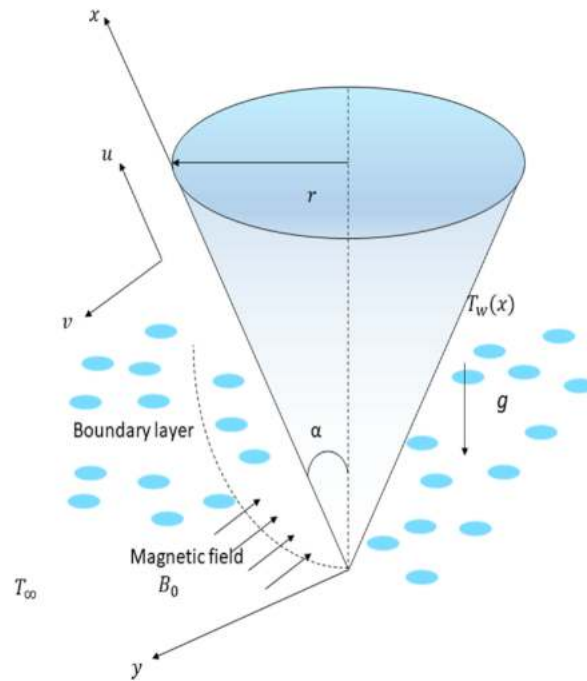


Fig. 1. Graphical model.

employed for any Prandtl number.

The Crank-Nicolson scheme (CNS) is a finite difference technique utilised in numerical analysis to resolve different classes of partial differential equations like the heat equation. Zubair et al. [58] employed the CNS to explore the fractional-order unsteadiness HNFs movement of natural convective flow of viscous liquids. Bejawada et al. [59] optimised a chemical reaction and viscous dissipation flowing of magnetic HNFs via natural convection by engaging CNS. Hanif [60,61] analyzed HT in Maxwell fluid using CNS assisted by Caputo fractional derivatives. Soomro et al. [62] studied the Brownian motion and thermophoretic effects on HNFs movement via CNS. Salilhet al. [63] proposed a numerical CNS fleeting current analysis of a heat exchanger filled with stage alteration material. To the best of the author’s knowledge, this could be the fresh attempt with the Crank-Nicolson scheme (CNS) to explore the hybrid nanofluid efficiency over a vertical cone. Many industrial and manufacturing processes encounter such kind of situation, which needs research attention. Places like lath works, metal stamping, drilling and material crafting, etc., may engage conical structures with heat that should be cooled for better performance. To some extent, this work was framed based on such inspiration with trending heat-efficient fluid and better schemes as tools. It is expected that the applications in nature and engineering for our research include the design of a ventilated heating structure, the preservation of electrical parts, and the design of a blood oxygenator and various including the design of a ventilated heating structure, the cooling of microelectronic apparatuses, and the proposal of a blood oxygenator and multiple kinds of agricultural products (grain and food).

2. Problem description

Consider a hybrid nanofluid ($Fe_3O_4-Cu/water$) with the velocity $u_w(x/L)$ is flowing over a vertical cone having variable wall temperature $T_w(x)$ inside porous medium. The surface of the cone is taken as x - axis, and the y - axis is presumed in the perpendicular orientation to the flowing, see Fig. 1. An outward magnetic field of strength ($B = B_0 + B_1$) is the affected perpendicular to the flowing path in the occurrence of thermal radiative flux. The induced magnetic field (B_1) can be insignificant because the magnetic Reynolds number is thought to be too small. The viscosity of the fluid assumed to be temperature dependent. Using boundary layer considerations and Boussinesq approximations, the constitutive formulas for the flow action of a hybrid nanofluid are developed as (Fig. 1):

$$\frac{\partial}{\partial x}(ru) + \frac{\partial}{\partial y}(rv) = 0, \tag{1}$$

$$\rho_{hmf} \left(\frac{\partial u}{\partial t} + u \frac{\partial u}{\partial x} + v \frac{\partial u}{\partial y} \right) = \frac{\partial}{\partial y} \left(\mu(T) \frac{\partial u}{\partial y} \right) - \frac{\mu(T)}{k_0} u - \sigma_{hmf} B_0^2 u + g(\rho\beta)_{hmf} (T - T_\infty) \cos \alpha, \tag{2}$$

$$(\rho C_p)_{hmf} \left(\frac{\partial T}{\partial t} + u \frac{\partial T}{\partial x} + v \frac{\partial T}{\partial y} \right) = k_{hmf} \frac{\partial^2 T}{\partial y^2} - \frac{\partial q_r}{\partial y}, \tag{3}$$

depending on the initially boundary constraints:

Table 1
Mathematical representations of nanofluid and hybridity nanofluid (Jamshed et al. [7] and Hanif et al. [22]).

Property	Nanofluid	Hybridity nanofluid
Viscosity	$\mu_{nf} = \frac{\mu_f}{(1 - \varphi_{p_1})^{2.5}}$	$\mu_{hnf} = \frac{\mu_{nf}}{(1 - \varphi_{p_2})^{2.5}}$
Density	$\rho_{nf} = (1 - \varphi_{p_1})\rho_f + \varphi_{p_1}\rho_{p_1}$	$\rho_{hnf} = (1 - \varphi_{p_2})\rho_{nf} + \varphi_{p_2}\rho_{p_2}$
Thermal expansion	$(\rho\beta)_{nf} = (1 - \varphi_{p_1})(\rho\beta)_f + \varphi_{p_1}(\rho\beta)_{p_1}$	$(\rho\beta)_{hnf} = (1 - \varphi_{p_2})(\rho\beta)_{nf} + \varphi_{p_2}(\rho\beta)_{p_2}$
Heat capacitance	$(\rho C_p)_{nf} = (1 - \varphi_{p_1})(\rho C_p)_f + \varphi_{p_1}(\rho C_p)_{p_1}$	$(\rho C_p)_{hnf} = (1 - \varphi_{p_2})(\rho C_p)_{nf} + \varphi_{p_2}(\rho C_p)_{p_2}$
Thermal conductivity	$k_{nf} = \frac{(k_{p_1} + 2k_f) + 2\varphi_{p_1}(k_{p_1} - k_f)}{(k_{p_1} + 2k_f) - \varphi_{p_1}(k_{p_1} - k_f)}$	$k_{hnf} = \frac{(k_{p_2} + 2k_{nf}) + 2\varphi_{p_2}(k_{p_2} - k_{nf})}{(k_{p_2} + 2k_{nf}) - \varphi_{p_2}(k_{p_2} - k_{nf})} \times k_{nf}$
Electrical conductivity	$\frac{\sigma_{nf}}{\sigma_f} = 1 + \frac{3\varphi_{p_1} \left(\frac{\sigma_{p_1} - 1}{\sigma_f} \right)}{\left(\frac{\sigma_{p_1} + 2}{\sigma_f} \right) - \varphi_{p_1} \left(\frac{\sigma_{p_1} - 1}{\sigma_f} \right)}$	$\sigma_{hnf} = \frac{(\sigma_{p_2} + 2\sigma_{nf}) + 2\varphi_{p_2}(\sigma_{p_2} - \sigma_{nf})}{(\sigma_{p_2} + 2\sigma_{nf}) - \varphi_{p_2}(\sigma_{p_2} - \sigma_{nf})} \times \sigma_{nf}$

$$\begin{aligned}
 u(x, y, 0) = 0, v(x, y, 0) = 0, T(x, y, 0) = T_\infty, \\
 u(0, y, t) = 0, T(0, y, t) = T_\infty, \\
 u(x, 0, t) = u_w(x/L), v(x, 0, t) = 0, T(x, 0, t) = T_w(x), \\
 u(x, \infty, t) = 0, T(x, \infty, t) = T_\infty.
 \end{aligned} \tag{4}$$

Here $r, \rho, k_0, \mu, \sigma, g, \beta, C_p, k, q_r$ and the subscript hnf represent radius of the cone, density, permeability of porous medium, dynamic viscosity, electrical conductivity, acceleration due to gravity, volumetric thermal expansion, heat capacity at fixed pressure, thermal conductivity, radiative heat flux and hybrid nanofluid, correspondingly. The mathematical formulas for hybrid nanofluid characteristics are organized in Table 1.

3. Non-dimensional model

Non-dimensional parameters are used to simplify the computing process by allowing all units of each parameter and variable to be discarded (see Table 2). The dimensionless factors listed below are established:

$$x^* = \frac{x}{L}, y^* = y \left(\frac{u_w}{\nu_f L} \right)^{\frac{1}{2}}, r^* = \frac{r}{L}, t^* = \frac{u_w t}{L}, u^* = \frac{u}{u_w}, v^* = v \left(\frac{u_w \nu_f}{L} \right)^{-\frac{1}{2}}, T^* = \frac{T - T_\infty}{T_w - T_\infty}. \tag{5}$$

In equation (2), the temperature dependent viscosity varies exponentially (Reynolds exponential viscosity model) and defined as

$$\mu(T) = \mu_{hnf} e^{-A(T - T_\infty)}, \tag{6}$$

where A is the strength dependence involving temperature (T) and viscosity (μ). Applying Maclaurin's expansion and dimensionless parameters (5) in equation (6) yields us to:

$$\mu(T) \cong \mu_{hnf}(1 - \gamma T), \tag{7}$$

here $\gamma = A(T_w - T_\infty)$ represents the viscosity variation parameter. With the help of nondim vari2,eq:viscosity, the non-dimensional form of equations (1)–(3) are obtained as

$$\frac{\partial(ru)}{\partial x} + \frac{\partial(rv)}{\partial y} = 0, \tag{8}$$

$$\varphi_1 \left(\frac{\partial u}{\partial t} + u \frac{\partial u}{\partial x} + v \frac{\partial u}{\partial y} \right) = \varphi_2 (1 - \gamma T) \left[\frac{\partial u^2}{\partial y^2} - \frac{1}{K} u \right] - \varphi_2 \gamma \frac{\partial T}{\partial y} \frac{\partial u}{\partial y} - \varphi_3 M u + \varphi_4 Ri T \cos \alpha, \tag{9}$$

$$\varphi_5 \left(\frac{\partial T}{\partial t} + u \frac{\partial T}{\partial x} + v \frac{\partial T}{\partial y} \right) = \frac{(\varphi_6 + Rd)}{Pr} \frac{\partial^2 T}{\partial y^2}. \tag{10}$$

subject to

$$\begin{aligned}
 u(x, y, 0) = 0, \quad v(x, y, 0) = 0, \quad T(x, y, 0) = 0, \\
 u(0, y, t) = 0, \quad T(0, y, t) = 0, \\
 u(x, 0, t) = x, \quad v(x, 0, t) = 0, \quad T(x, 0, t) = x^n, \\
 u(x, \infty, t) = 0, \quad T(x, \infty, t) = 0.
 \end{aligned} \tag{11}$$

Here $\varphi_1 = \frac{\rho_{hmf}}{\rho_f}$, $\varphi_2 = \frac{\mu_{hmf}}{\mu_f}$, $\varphi_3 = \frac{\sigma_{hmf}}{\sigma_f}$, $\varphi_4 = \frac{(\rho\beta)_{hmf}}{(\rho\beta)_f}$, $\varphi_5 = \frac{(\rho C_p)_{hmf}}{(\rho C_p)_f}$, $\varphi_6 = \frac{k_{hmf}}{k_f}$, $\frac{1}{K} = \frac{\nu_f L}{k_0 u_w}$, $M = \frac{\sigma_f B_0^2 L}{\rho_f \mu_w}$, $Ri = \frac{g\beta(T_w - T_\infty)L}{u_w^2}$, $Rd = \frac{16\sigma_b T_\infty^3}{3k_b k_f}$ and $Pr = \frac{(\mu C_p)_f}{k_f}$.

4. Physical properties

The physical properties of attraction like Nusselt number (Nu_x) and frictional force (C_f) are distinguished as

$$Nu_x = \frac{xq_w}{k_f(T_w - T_\infty)}, C_f = \frac{\tau_w}{\rho_f u_w^2}. \tag{12}$$

where $q_w = -k_{hmf} \left(\frac{\partial T}{\partial y}\right)_{y=0}$ and $\tau_w = \mu(T) \left(\frac{\partial u}{\partial y}\right)_{y=0}$ are the wall heat flux and wall shear stress, respectively. The dimensionless form of above physical quantities are given by

$$Nu_x Re^{-1/2} = -\varphi_6 x \left(\frac{\partial T}{\partial y}\right)_{y=0}, C_f Re^{1/2} = \varphi_2 (1 - \gamma T) \left(\frac{\partial u}{\partial y}\right)_{y=0}. \tag{13}$$

5. Entropy generation analysis

Let us introduce entropy generated by heat transfer (*HFI*) and entropy generated by fluid friction (*FFI*):

$$HFI = \frac{k_{hmf}}{T_\infty^2} \left(1 + \frac{16\sigma_b T_\infty^3}{k_b k_{hmf}}\right) \left[\frac{\partial T}{\partial y}\right]^2, \tag{14}$$

$$FFI = \frac{\mu(T)}{T_\infty} \left[\left(\frac{\partial u}{\partial y}\right)^2 + \frac{1}{K} u^2\right] + \frac{\sigma_{hf} B_0^2}{T_\infty} u^2. \tag{15}$$

In equation (11), first term is the entropy generating as a result of viscous dissipation, second term is caused by porous medium and third term is by reason of magnetic field. The total entropy generation (S_{gen}) is

$$S_{gen} = HFI + FFI, \\ = \frac{k_{hmf}}{T_\infty^2} \left(1 + \frac{16\sigma_b T_\infty^3}{k_b k_{hmf}}\right) \left(\frac{\partial T}{\partial y}\right)^2 + \frac{\mu(T)}{T_\infty} \left[\left(\frac{\partial u}{\partial y}\right)^2 + \frac{1}{K} u^2\right] + \frac{\sigma_{hf} B_0^2}{T_\infty} u^2. \tag{16}$$

The nondimensional entropy production S_{GEN} is described as the proportion of the volumetric entropy production (S_{gen}) to the property of entropy rate (S_0). Mathematically

$$S_{GEN} = \frac{S_{gen}}{S_0} = (\varphi_6 + Rd) \left(\frac{\partial T}{\partial y}\right)^2 + \varphi_2 Br \Omega^{-1} (1 - \gamma T) \left[\left(\frac{\partial u}{\partial y}\right)^2 + \frac{1}{K} u^2\right] + \varphi_3 Br \Omega^{-1} Mu^2, \tag{17}$$

provided that

$$S_0 = \frac{k_f (T_w - T_\infty)^2 u_w}{T_\infty^2 \nu_f L}, Br = \frac{\mu_f u_w^2}{k_f (T_w - T_\infty)}, \Omega = \frac{T_w - T_\infty}{T_\infty}. \tag{18}$$

Let N_1 and N_2 signify the irreversibility as a result of heat transference and fluid resistance, correspondingly, then equation (17) gets the formula

$$S_{GEN} = N_1 + N_2, \tag{19}$$

given that

$$N_1 = (\varphi_6 + Rd) \left(\frac{\partial T}{\partial y}\right)^2, N_2 = \varphi_2 Br \Omega^{-1} (1 - \gamma T) \left[\left(\frac{\partial u}{\partial y}\right)^2 + \frac{1}{K} u^2\right] + \varphi_3 Br \Omega^{-1} Mu^2. \tag{20}$$

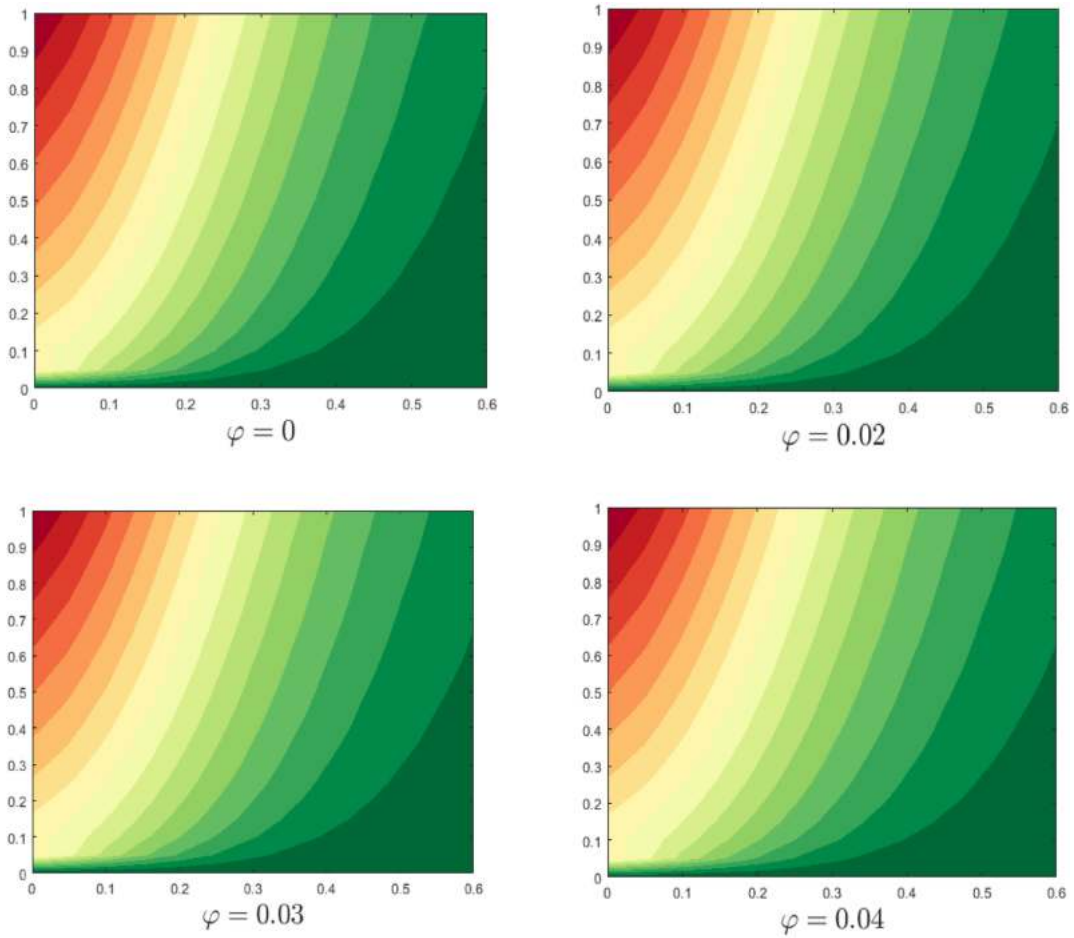
The Bejan number (*Be*) is worthy for estimating irreversibility profile. It is defined as the ratio of entropy creation owing to heat transference to whole entropy production

$$Be = \frac{N_1}{N_1 + N_2}. \tag{21}$$

The Bejan number has a range of [0, 1]. $Be = 0$ specifies that N_1 is overcome by N_2 , but $Be = 1$ indicates that N_1 is controlled by N_2 . If the entropy produced by fluid resistance and heat transference provide equivalently, the *Be* amount is 0.5.

6. Numerical procedure: Crank–Nicolson method

The Crank–Nicolson approach, which resembles the formulas at the present and forward time levels on average, i.e., n^{th} and



(a). Entropy generating for φ when $K = 0.5, M = 3, Rd = 0.5, \gamma = 0.1,$ and $n = 0.25$

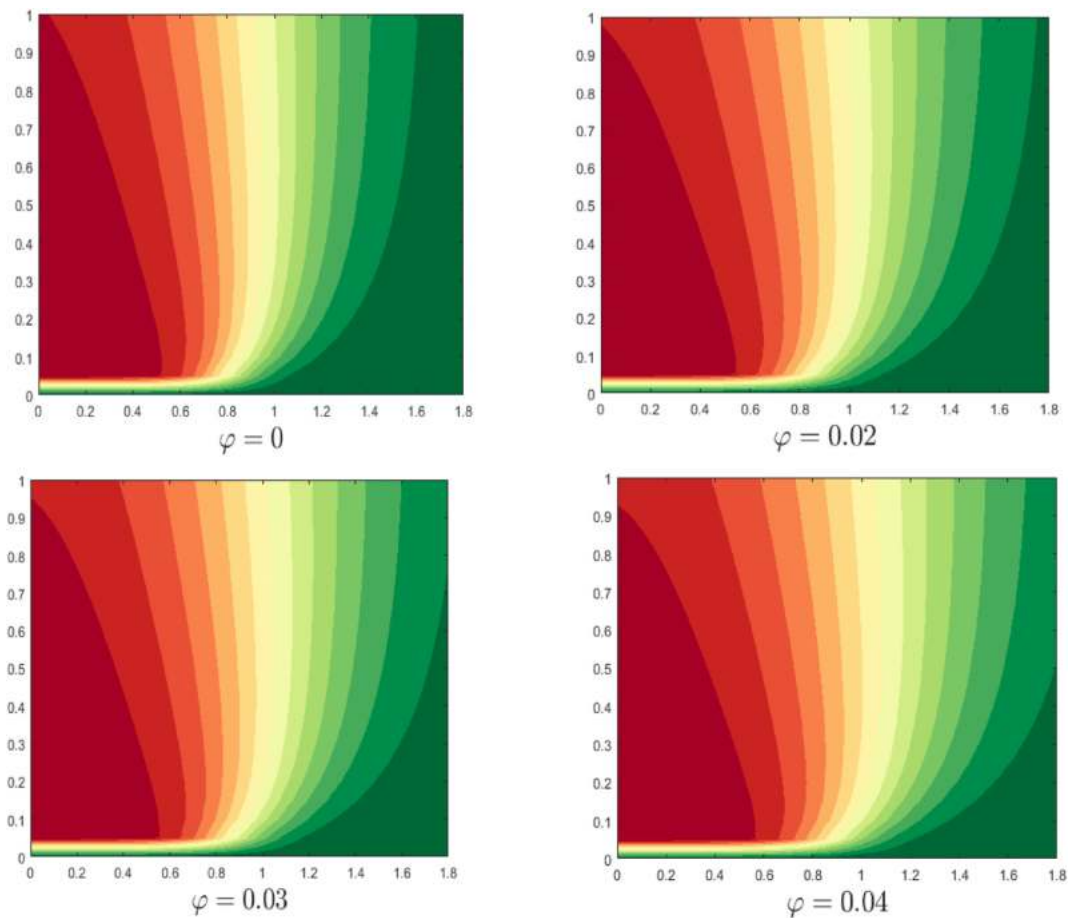
Fig. 2a. Entropy generating for when $K = 0.5, M = 3, Rd = 0.5, \gamma = 0.1,$ and $n = 0.25$.

$(n + 1)^{th}$ time level, is employed to estimate the derivative terms in equations 8–11. Let u_{ij}^n, v_{ij}^n and T_{ij}^n be the computational approximations of $u(x, y, t), v(x, y, t),$ and $T(x, y, t)$ at time n for any pair (x_i, y_j) .

$$\frac{u_{ij-1}^{n+1} - u_{i-1,j-1}^{n+1} + u_{ij}^{n+1} - u_{i-1,j}^{n+1} + u_{ij-1}^n - u_{i-1,j-1}^n + u_{ij}^n - u_{i-1,j}^n}{4\Delta x} + \frac{v_{ij}^{n+1} - v_{ij-1}^{n+1} + v_{ij}^n - v_{ij-1}^n}{2\Delta y} = 0, \tag{22}$$

$$\begin{aligned} \varphi_1 \left(\frac{u_{ij}^{n+1} - u_{ij}^n}{\Delta t} + u_{ij}^n \frac{u_{ij}^{n+1} - u_{i-1,j}^{n+1} + u_{ij}^n - u_{i-1,j}^n}{2\Delta x} \right. \\ \left. + v_{ij}^n \frac{u_{ij+1}^{n+1} - u_{ij-1}^{n+1} + u_{ij+1}^n - u_{ij-1}^n}{4\Delta y} \right) = \varphi_2 \left(1 - \gamma \frac{T_{ij}^{n+1} + T_{ij}^n}{2} \right) \left(\frac{u_{ij+1}^{n+1} - 2u_{ij}^{n+1} + u_{ij-1}^{n+1} + u_{ij+1}^n - 2u_{ij}^n + u_{ij-1}^n - u_{ij}^{n+1} + u_{ij}^n}{2\Delta y^2} - \frac{u_{ij}^{n+1} + u_{ij}^n}{2K} \right) \\ - \varphi_2 \gamma \left(\frac{T_{ij+1}^{n+1} - T_{ij-1}^{n+1} + T_{ij+1}^n - T_{ij-1}^n}{4\Delta y} \right) \left(\frac{u_{ij+1}^{n+1} - u_{ij-1}^{n+1} + u_{ij+1}^n - u_{ij-1}^n}{4\Delta y} \right) \\ - \varphi_3 M \left(\frac{u_{ij}^{n+1} + u_{ij}^n}{2} \right) + \varphi_4 Ri \left(\frac{T_{ij}^{n+1} + T_{ij}^n}{2} \right) \cos \alpha, \end{aligned} \tag{23}$$

$$\varphi_5 \left(\frac{T_{ij}^{n+1} - T_{ij}^n}{\Delta t} + u_{ij}^n \frac{T_{ij}^{n+1} - T_{i-1,j}^{n+1} + T_{ij}^n - T_{i-1,j}^n}{2\Delta x} + v_{ij}^n \frac{T_{ij+1}^{n+1} - T_{ij-1}^{n+1} + T_{ij+1}^n - T_{ij-1}^n}{4\Delta y} \right) = \frac{\varphi_6 + Rd}{Pr} \left(\frac{T_{ij+1}^{n+1} - 2T_{ij}^{n+1} + T_{ij-1}^{n+1} + T_{ij+1}^n - 2T_{ij}^n + T_{ij-1}^n}{2\Delta y^2} \right). \tag{24}$$



(b). Bejan number for φ when $K = 0.5, M = 3, Rd = 0.5, \gamma = 0.1,$ and $n = 0.25.$

Fig. 2b. Bejan number for φ when $K = 0.5, M = 3, Rd = 0.5, \gamma = 0.1,$ and $n = 0.25.$

The computational solution was obtained using the mesh size $(\Delta x, \Delta y) = (0.05, 0.05)$ in the (x, y) orientation and the time level $(\Delta t = 0.01)$. Numerous computational iterations are done to achieve convergence solutions, which are assumed to be reached when the absolute error for all grid nodes tackles 1×10^{-5} .

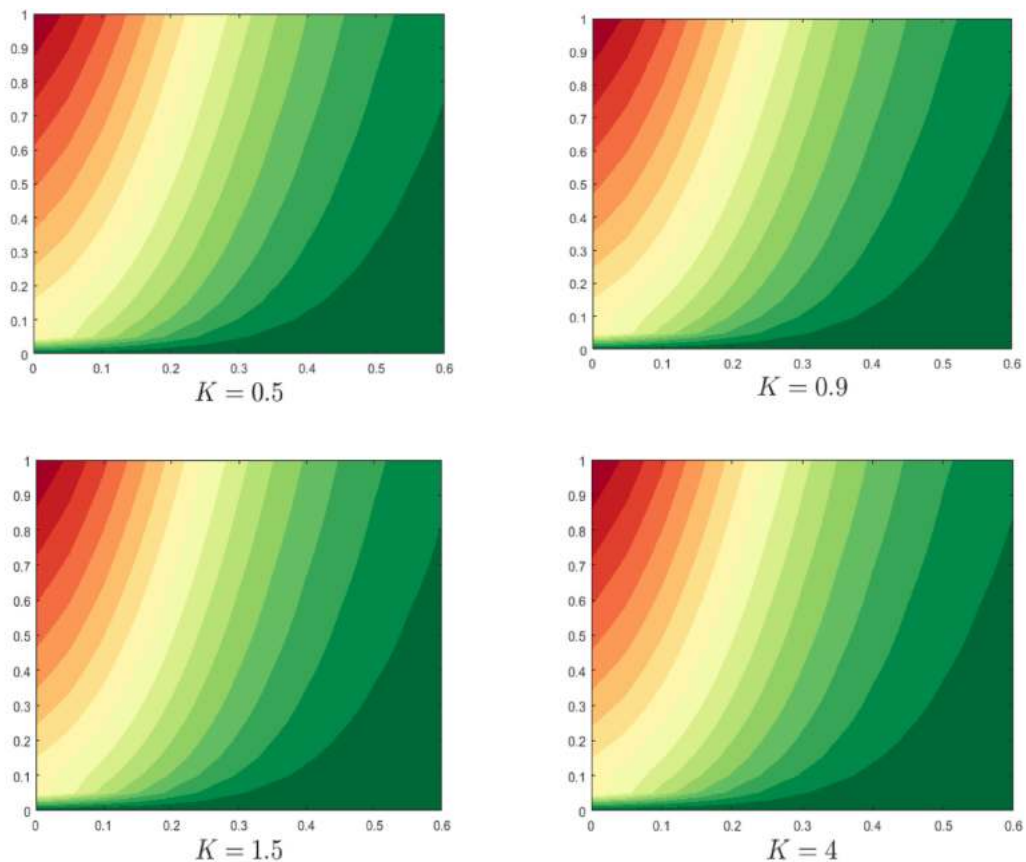
7. Graphical results and discussion

Study based on vertically porous cone flow of Fe_3O_4 -Cu/water hybrid nanofluid with varying viscosity to explore the entropy, frictional factor, and heat transfer aspects under thermal radiation and hydromagnetic influences. Results of the parametrical study based on fractional volume φ ($0 \leq \varphi \leq 0.04$), magnetic M ($0 \leq M \leq 4$), viscosity variation γ ($0 \leq \gamma \leq 0.5$), permeability K ($0.5 \leq K \leq 4.5$), and thermal radiation Rd ($0 \leq Rd \leq 4$) constraints were revealed in the forms of plots from Figs. 2-5 for entropy variations and Bejan number along with the graphical plots from Figs. 6 and 7 and tabular display Table 3 for friction factor and Nusselt number (Nu).

7.1. Fractional volume (φ) impacts

Fig. 2(a) highlights the entropy changes that happened around the vertical cone due to fractional volume (φ) alteration in the Fe_3O_4 -Cu/water hybrid nanofluid. By increasing the fractional size of nanoparticles, the entropy lines begin to gradually spread away from the cone, as evidenced by the fact that the entropy lines begin to move away from the cone when the fractional size of nanoparticles is increased. This may be because a larger area of the cone was exposed to the fluid flow on the higher side compared to the base end. This suggests that the flow of fluid may not be evenly distributed throughout the cone, and further investigation is needed to determine the cause of this uneven distribution. Additionally, adjustments to the design or placement of the cone may be necessary to minimize entropy losses. Change in φ exhibits the nominal impact on the entropy changes.

Bejan contour varies from level 0 to 1 which is the ratio of the entropy generating through frictional factors and heat transference. $Be = 0$ reflects the dominance of heat transference-based entropy losses (N_1) over the other. Around $Be = 0.5$, the contribution towards the entropy tends to be equal from both factors. For higher-end Bejan number values, $Be = 1$, the entropy due to frictional



(a). Entropy generating for K when $\varphi = 0.01$, $M = 3$, $Rd = 0.5$, $\gamma = 0.1$, and $n = 0.25$.

Fig. 3a. Entropy generating for K when $\varphi = 0.01$, $M = 3$, $Rd = 0.5$, $\gamma = 0.1$, and $n = 0.25$.

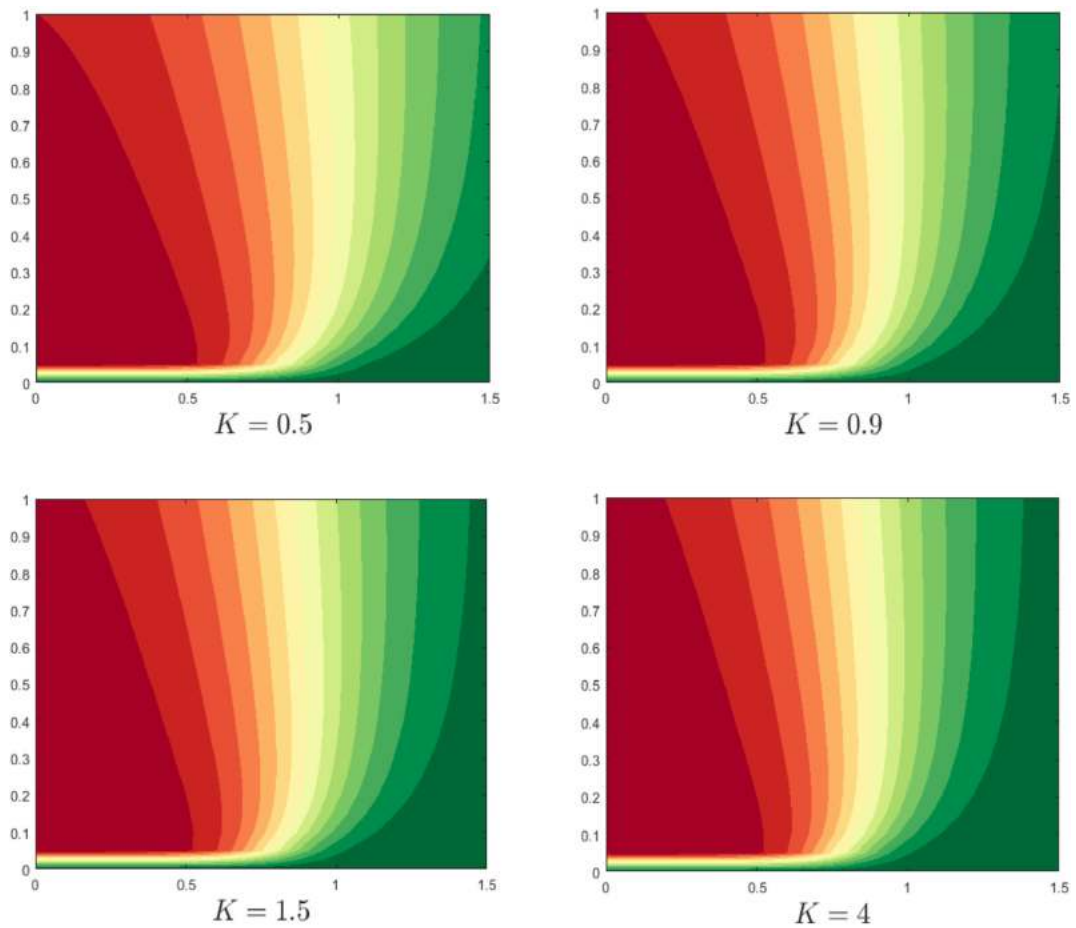
factors dominated the heat transfer-induced entropy losses. Bejan lines (*Be*) for the diverse amounts of φ can be visualized in Fig. 2(b). With the growth of the amount of φ , the Bejan outlines begin to expand little by little away from the cone more clearly and significantly more than in the case of entropy. A higher volume fraction favours the heat transference ability of the liquid, which technically raises the entropy loss due to thermal transference. This can be visualized in Fig. 2(b), where the Bejan lines for the higher fractional volume get reduced where the total entropy dominates the ratio. In other words, enhancing the fractional size φ of the liquid results in a more efficient heat transfer process, as less entropy is lost during thermal transfer. This finding has important implications for the design and optimisation of heat exchangers and other thermal management systems.

7.2. Porosity impacts

Porosity (K) plays a vital role in flow, thermal, and entropy alterations by regulating the fluid movements in the system. Fig. 3(a–b) evident the nominal impact of porosity over the entropy generating and Bejan curves. It is remarked that by boosting the values of K , the entropy outlines begin to gather near the cone. While the growth of the values of K makes the Bejan outlines begin to collect near the cone more clearly and significantly more than in the situation of entropy, this may be because the vertical posture of the cone experiences minimal influence due to porosity when compared to the lateral cone flows. Generally, both the entropy and the Bejan lines get reduced as porosity increases, as the alteration in porosity works slightly against them. This observation suggests that porosity can play a significant role in the behaviour of fluid flows and their associated thermodynamic properties. Supplementary examination is needed to fully comprehend the impact of porosity on entropy and Bejan lines in different flow scenarios.

7.3. Magnetic impacts

Fig. 4(a–b) portray the interactive magnetic field (M) influences over the entropy generation and Bejan line respectively in the system. It is noted that by swelling of M values, the entropy and Bejan outlines deviate far from the cone but in the situation of Bejan, the deviation is significantly more than in the situation of entropy. Fig. 4. (a) illustrates the overall entropy losses that result from the magnetic interaction slowing down the Lorentz force-induced fluid flow while also reducing the heat transfer process. In terms of Bejan



(b). Bejan number for K when $\varphi = 0.01$, $M = 3$, $Rd = 0.5$, $\gamma = 0.1$, and $n = 0.25$.

Fig. 3b. Bejan number for K when $\varphi = 0.01$, $M = 3$, $Rd = 0.5$, $\gamma = 0.1$, and $n = 0.25$.

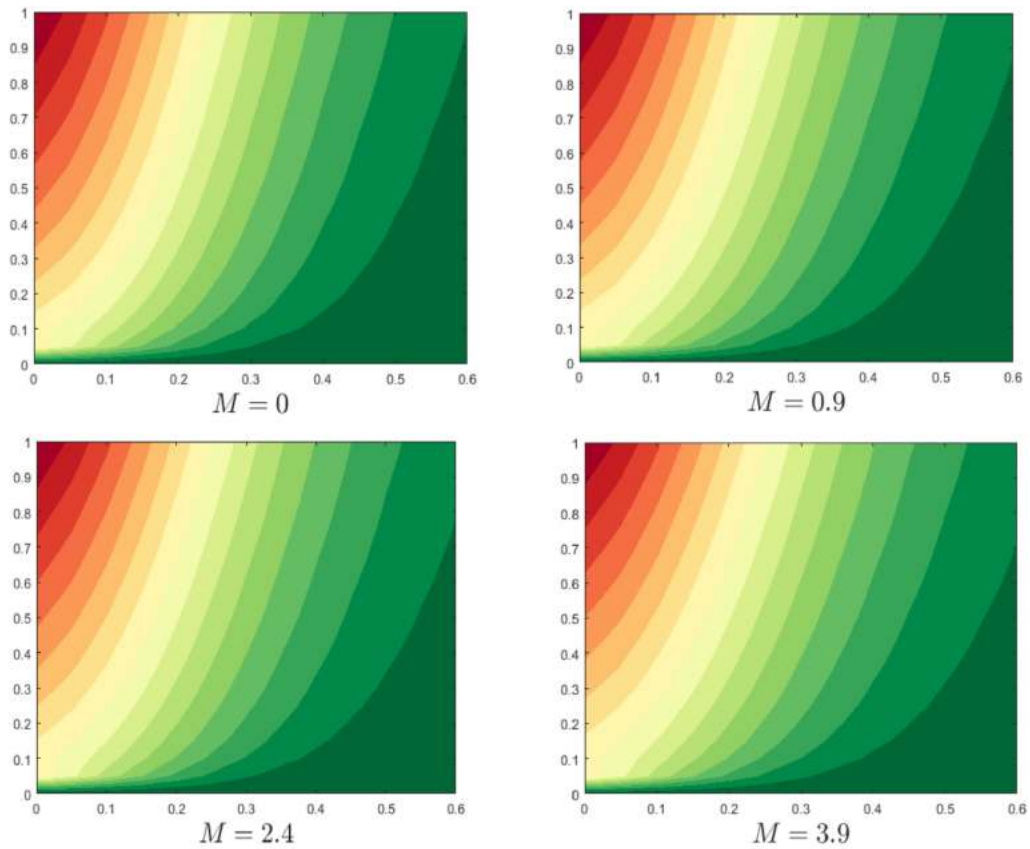
lines, the magnetic interaction constraint has a significant impact on the amount that can be reduced. In order to achieve higher magnetic interactions, Bejan contours were simplified. It's possible that this is due to the dominance of total entropy overheat transfer entropy production, which is restricted as a result of magnetic interaction. This finding could have implications for the design of more efficient magnetic devices, as simplifying Bejan contours may lead to improved magnetic interactions and, ultimately, greater energy savings.

7.4. Impacts of viscous variation

Fig. 5(a–b) disclose the effect of viscous variations (γ) on irreversible energy losses in the form of entropy generation and Bejan variations respectively. It is noted that by rising of γ values, the entropy outlines swerve far from the cone sparsely. Likewise, the incrementation of the amounts of γ makes the Bejan outlines begin to diverge away from the cone more clearly and notably more than in the situation of entropy outlines. However, while the viscid variation has nominal control over the entropy, it gets better as it moves further from the base of the vertical surface, as can be seen in Fig. 5(a). When the viscosity of the liquid increases, the fluidity decreases, most noticeably towards the top of the vertical cone, making it more difficult to navigate. This type of slower flow may help to grab more heat from the surface, which raises entropy as a result of heat transference and can be seen in Fig. 5(b) as the Bejan lines. This phenomenon is commonly observed in high viscosity fluids such as honey or molasses. Understanding the relationship between viscosity and fluidity is crucial in various fields, such as chemical engineering and material science.

7.5. Nusselt number (Nu) for fractional volume (φ) and porosity

The enhance in the Nusselt amount that can be established in Fig. 6(a) is a reflection of the fact that the fractional volume has been improved, which means that the nanofluid is becoming more effective at facilitating the heat transference process. In the meantime, higher porosity works in favour of more fluid movement within the system, which also switches on the heat transfer process in a positive way. This is shown in the increased Nusselt number in Fig. 6(a), which shows that the operation was successful. The results



(a). Entropy generating for M when $\varphi = 0.01$, $K = 0.5$, $Rd = 0.5$, $\gamma = 0.1$, and $n = 0.25$.

Fig. 4a. Entropy generating for M when $\varphi = 0.01$, $K = 0.5$, $Rd = 0.5$, $\gamma = 0.1$, and $n = 0.25$.

suggest that both porosity and fluid movement play crucial roles in enhancing the heat transfer process. Therefore, optimising these factors can lead to more efficient heat transfer systems.

7.6. Nusselt number (Nu) for magnetic and radiation constraints

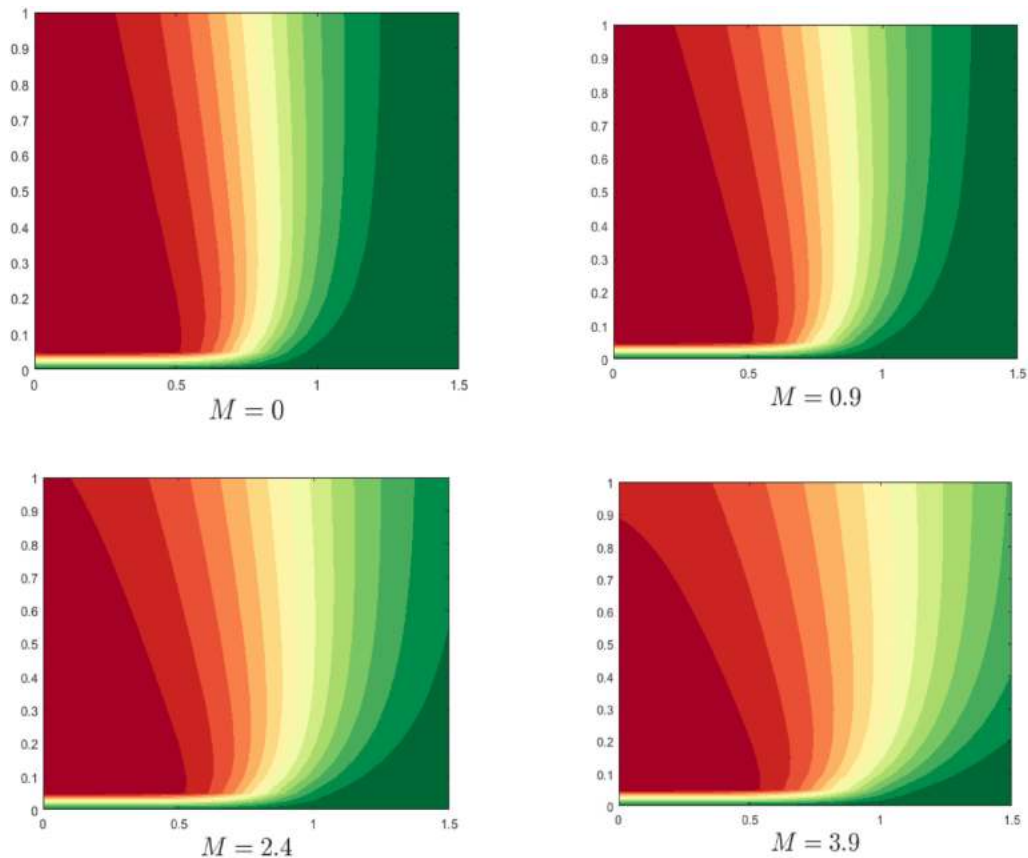
The magnetic interaction slows down the heat transfer in the scheme because it impedes the flow motion in the system, which is a direct result of the magnetic interaction. The decreased Nusselt amount shown in Fig. 6(b) provides evidence for the earlier conclusion that magnetic strength has improved. Concurrently, larger values of radiation constraint raise the heat in the system as a result of the additional heat from the radiating body. This has the effect of working against the rate at which heat is transferred. A scenario like this one, with a lower Nusselt number for higher thermal radiation, is depicted in Fig. 6(c). In other words, the higher the thermal radiation, the more difficult it becomes for heat to be transferred efficiently. This phenomenon is important to consider in various industrial and engineering applications where heat transfer is a critical factor.

7.7. Skin friction for fractional volume (φ) and porosity

The changes in frictional resistance that occurred in the system as a result of the porosity and volume fraction are shown in Fig. 7 (a). It should be pointed out that because of the porous resistance, it helps to elevate the skin friction, while the volume fraction tends to minimize it. This may be observed. The enhanced flow that resulted from the increasing porosity and the fractionally added particle strength in the flowing fluid was the factor that was responsible for such trends. Therefore, it can be concluded that the combination of porous resistance and volume fraction has a significant impact on skin friction and flow enhancement. These findings can have practical applications in various fields, such as aerospace engineering and fluid dynamics.

7.8. Skin friction for magnetic and radiation constraints

Even though it is technically a slower flow, it entails very little frictional resistance. The flow is slowed down as a result of magnetic interaction with the flow, which is reflected in lower skin friction in Fig. 7(b). Fig. 7(c), on the other hand, demonstrates that the flow of the warmer fluid that has been subjected to radiation heat moves faster than it did in the normal state, which increases the amount of



(b). Bejan number for M when $\varphi = 0.01$, $K = 0.5$, $Rd = 0.5$, $\gamma = 0.1$, and $n = 0.25$.

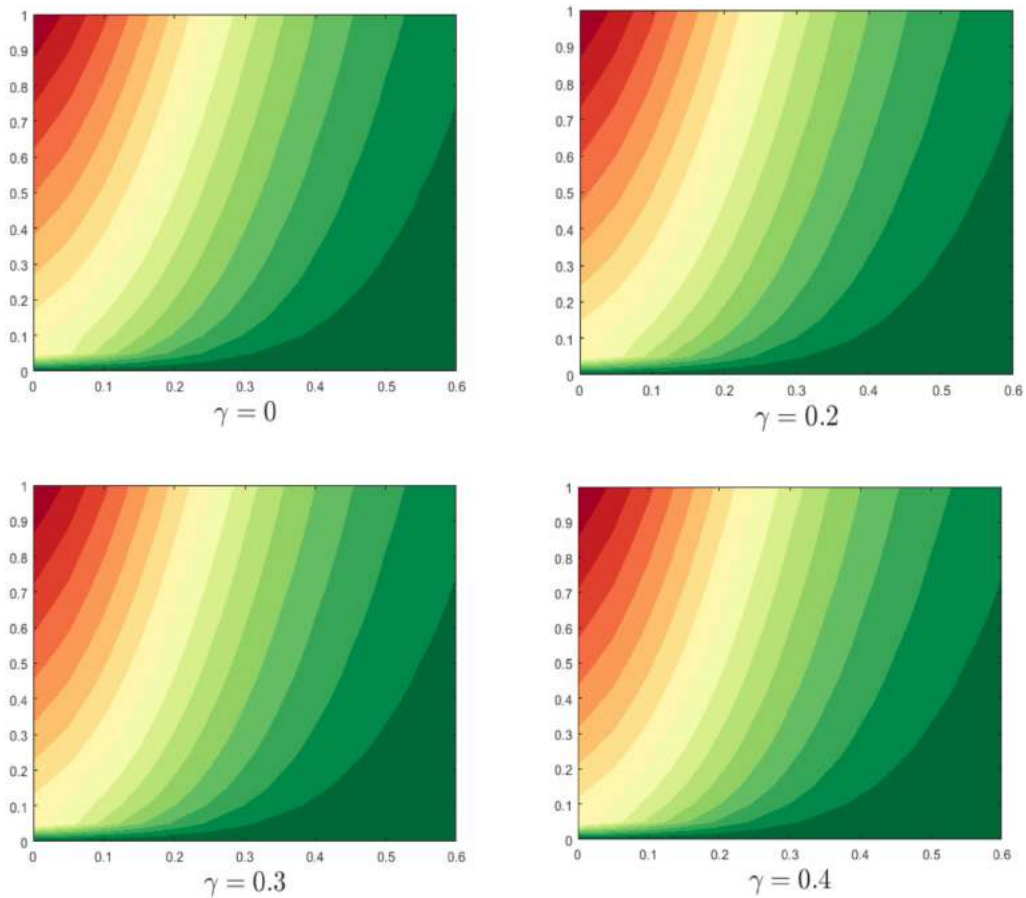
Fig. 4b. Bejan number for M when $\varphi = 0.01$, $K = 0.5$, $Rd = 0.5$, $\gamma = 0.1$, and $n = 0.25$.

friction that exists around the cone and in the flow system. Viscosity has a direct relationship to the frictional properties of a substance. Fig. 7(d) demonstrates that there is an increase in surface friction in reaction to an upsurge in the viscosity variation parameter. This increase in surface friction can cause a decline in the flow rate and an upsurge in pressure drop, which can affect the efficiency of the system. Therefore, it is important to consider the viscosity of substances when designing and optimising flow systems.

Table 3 highlights the computational display of the Nusselt amount and the frictional force in the system based on a parametrical analysis. Both of these results were obtained from the system. Porosity and radiation, two components that were helping flow in the system, had a tendency to raise frictional factors more than fractional volume and magnetic interactions, as can be observed from the graphical representations. The Nusselt number increased as a result of factors such as volume fraction and porosity that acted in favour of heat transport inside the systems. Alternatively, the Nusselt number decreased as a result of magnetic interaction and thermal radiation. Because developed viscosity inhibits heat transmission, the Nusselt number drops, and the surface friction increases with increasing viscosity parameters. On the other hand, lower viscosity parameters result in lower viscosity development. Therefore, it is important to carefully balance the magnetic interaction and thermal radiation with the viscosity parameters in order to optimise heat transmission in the system. This can lead to improved efficiency and performance in several industrial purposes, for instance heat exchangers and conserving systems.

8. Inference of the study

Numerical-based parametrical studies on varying viscous Fe_3O_4 -Cu/water hybrid nanofluid flow over the porous vertical cone subjected to thermal radiation and magnetic interactions. Features like entropy formation, skin friction, and heat transference rate were analyzed for the parameters such as fractional volume, Magnetic (M), Permeability (K), and Thermal radiation (Rd). The outcomes were visualized in the form of graphical plots and a table from which the following inferences were obtained.



(a). Entropy generating for γ when $\varphi = 0.01$, $K = 0.5$, $M = 3$, $Rd = 0.5$, and $n =$

0.25.

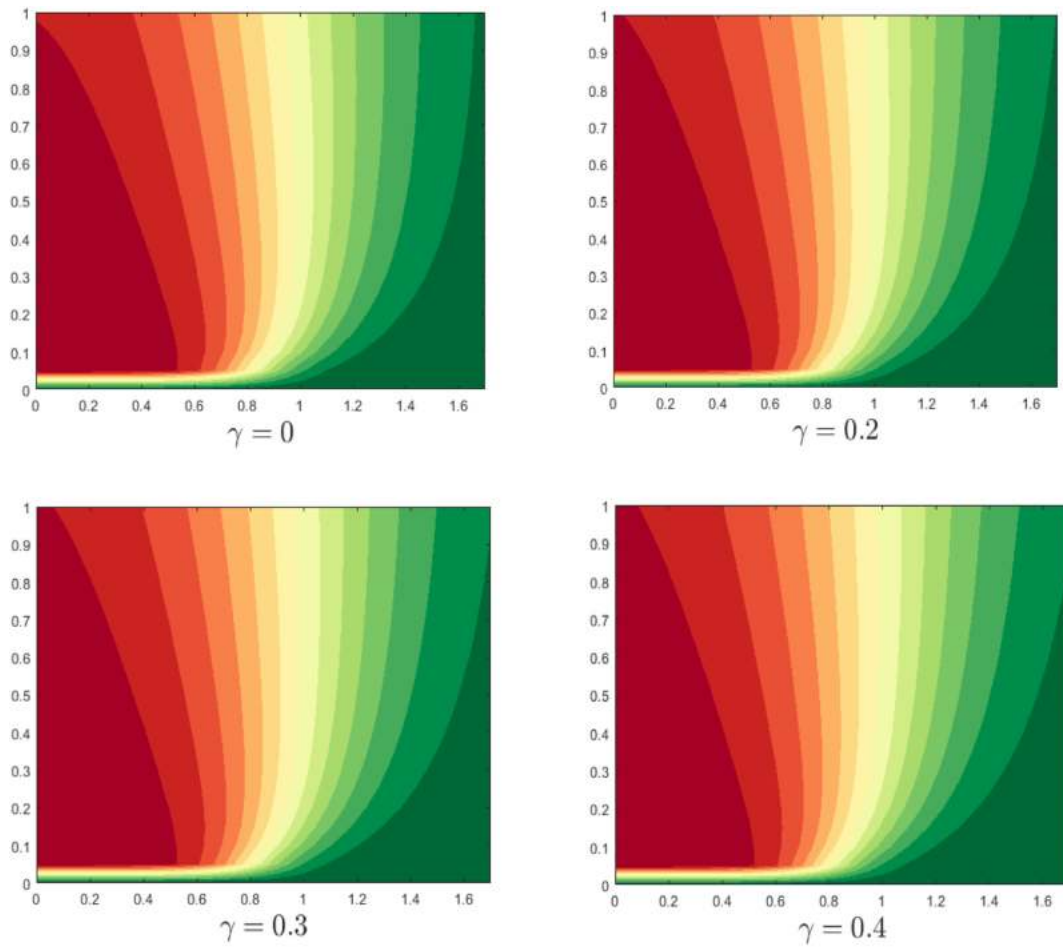
Fig. 5a. Entropy generating for γ when $\varphi = 0.01$, $K = 0.5$, $M = 3$, $Rd = 0.5$, and $n = 0.25$.

- Energy loss in the form of increased entropy can be noted at the further vertical end of the cone than the base.
- The parametrical influence was noted to be nominal when compared to the other physical aspects.
- Domination of heat transfer induced entropy generation and be observed for the porosity improvements.
- The magnetic interaction and volume fraction contribute more to the combined entropy than the heat transfer alone.
- Skin friction gets augmented for porosity, viscosity, and thermal radiation parameters and it gets reduced for fractional volume and magnetic interactions.
- Assisting factors like volume fraction and porosity elevates the heat transfer process as the magnetic interaction, viscosity, and thermal radiation stand against it.

In the forthcoming, the current procedure might be managed to a number of physical and specialised obstacles [64–72].

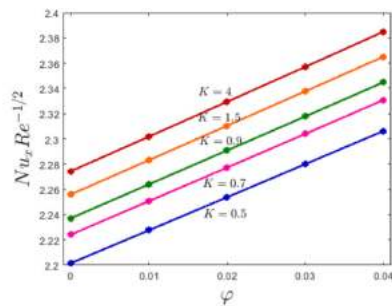
Declaration of competing interest

The authors declare that they have no known competing financial interests or personal relationships that could have appeared to influence the work reported in this paper.



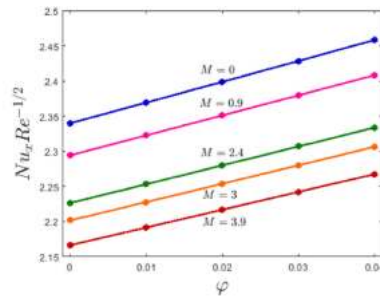
(b). Bejan number for γ when $\varphi = 0.01$, $K = 0.5$, $M = 3$, $Rd = 0.5$, and $n = 0.25$.

Fig. 5b. Bejan number for γ when $\varphi = 0.01$, $K = 0.5$, $M = 3$, $Rd = 0.5$, and $n = 0.25$.



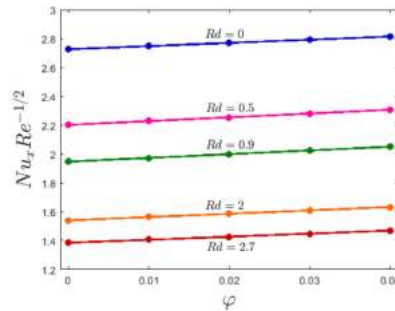
(a). Variational effects of K on Nusselt number for diverse values of φ when $M = 3$, $Rd = 0.5$, $\gamma = 0.1$, and $n = 0.25$.

Fig. 6a. Variational effects of K on Nusselt number for diverse values of φ when $M = 3$, $Rd = 0.5$, $\gamma = 0.1$, and $n = 0.25$.



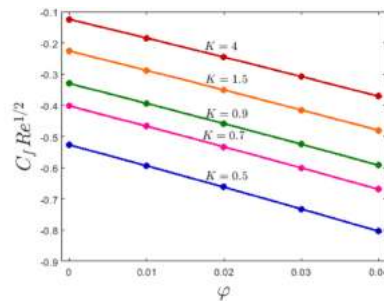
(b). Variational effects of M on Nusselt number for diverse values of φ when $K = 0.5$, $Rd = 0.5$, $\gamma = 0.1$, and $n = 0.25$.

Fig. 6b. Variational effects of M on Nusselt number for diverse values of φ when $K = 0.5$, $Rd = 0.5$, $\gamma = 0.1$, and $n = 0.25$.



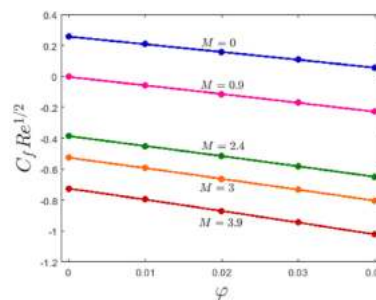
(c). Variational effects of Rd on Nusselt number for diverse values of φ when $K = 0.5$, $M = 3$, $\gamma = 0.1$, and $n = 0.25$.

Fig. 6c. Variational effects of Rd on Nusselt number for diverse values of φ when $K = 0.5$, $M = 3$, $\gamma = 0.1$, and $n = 0.25$.



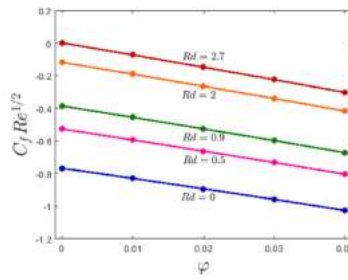
(a). Variational influences of K on the frictional force for diverse values of φ when $M = 3$, $Rd = 0.5$, $\gamma = 0.1$, and $n = 0.25$.

Fig. 7a. Variational influences of K on the frictional force for diverse values of φ when $M = 3$, $Rd = 0.5$, $\gamma = 0.1$, and $n = 0.25$.



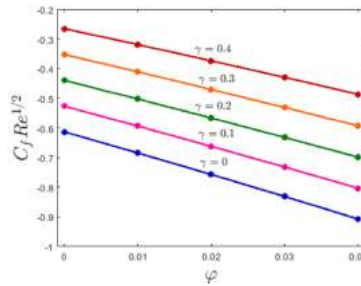
(b). Variational effects of M on the frictional force for diverse values of φ when $K = 0.5$, $Rd = 0.5$, $\gamma = 0.1$, and $n = 0.25$.

Fig. 7b. Variational effects of M on the frictional force for diverse values of φ when $K = 0.5$, $Rd = 0.5$, $\gamma = 0.1$, and $n = 0.25$.



(c). Variational effects of Rd on the frictional force for diverse values of ϕ when $K = 0.5, M = 3, \gamma = 0.1,$ and $n = 0.25$

Fig. 7c. Variational effects of Rd on the frictional force for diverse values of ϕ when $K = 0.5, M = 3, \gamma = 0.1,$ and $n = 0.25$.



(d). Variational effects of γ on the frictional force for diverse values of ϕ when $K = 0.5, M = 3, Rd = 0.5,$ and $n = 0.25$

Fig. 7d. Variational effects of γ on the frictional force for diverse values of ϕ when $K = 0.5, M = 3, Rd = 0.5,$ and $n = 0.25$.

Table 2
Thermophysical characteristics of pure water and nanomaterials.

Materials	$\rho(kgm^{-3})$	$\sigma(Sm^{-1})$	$\beta(K^{-1})$	$C_p(J kg^{-1}K^{-1})$	$k(Wm^{-1}K^{-1})$
Pure water	997.1	0.05	21×10^{-5}	4179	0.613
Fe_3O_4	5200	2.5×10^4	1.3×10^{-5}	670	6
Cu	8933	5.96×10^7	1.67×10^{-5}	385	401

Table 3
Nusselt number and skin friction coefficient for diverse governing variables.

ϕ	K	M	Rd	γ	$Nu_x Re^{-1/2}$	$-C_f Re^{1/2}$		
0	0.5	3	0.5	0.1	2.20152	0.52657		
0.01					2.22763	0.59363		
0.02					2.25378	0.66208		
0.03					2.27998	0.73199		
0.04					2.30622	0.80341		
0.01	0.7				2.2507	0.46675		
					0.9	2.26401	0.39369	
					1.5	2.28314	0.28779	
	4					2.30181	0.1845	
						0.5	2.36915	-0.208
						0.9	2.32248	0.05835
	3					2.25302	0.45058	
						2.4	2.19146	0.7962
						3.9	2.74744	0.82929
	0					0	1.97260	
						0.9	1.56277	0.19076
						2	1.40572	0.07284
	2.7					1.40572	0.07284	
						0	2.23074	0.68437
						0.2	2.22450	0.50231
0.3						2.22139	0.41057	
0.4					2.21839	0.31868		

Data availability

Data will be made available on request.

Acknowledgment

The authors extend their appreciation to the Deanship of Scientific Research at King Khalid University for funding this work through large group Research Project under grant number RGP2/251/44.

Nomenclature

(x,y)	Cartesian coordinates
(u,v)	velocity components in(x,y) direction
A	strength dependency
T	temperature
t	time
Nu_x	Nusselt number
C_f	Skin friction
Br	Brinkman number
Be	Bejan number
Re	Reynolds number
S_{GEN}	entropy generation
S_0	characteristic entropy rate
Δt	time step
Δx	grid size in x direction
Δy	grid size in y direction
Ω	temperature difference
k_0	permiability of porous medium
B	magnetic field strength
r	radius of the cone
Ri	Richardson number
k	thermal conductivity
g	gravitational accelration
K	non-dimensional porosity parameter
M	non-dimensional magnetic parameter
Rd	non-dimensional thermal radiation
L	reference length
C_p	specific heat capacity
Pr	Prandtl number
k_b	absorption parameter
σ_b	Steaften Boltzman coefficien
ρ	density
μ	dynamic viscosity
β	volumetric thermal expansion
α	cone angle
γ	viscosity variation
ν	kinematic viscosity
σ	electrical conductivity
φ	nanoparticles volume fraction
*	non-dimensional
f	base fluid
nf	nanofluid
hnf	hybrid nanofluid
p	nanoparticles
i	grid point in x direction
j	grid point in y direction
n	time level

References

- [1] M. Manzur, M. Khan, M. ur Rahman, Mixed convection heat transfer to cross fluid with thermal radiation: effects of buoyancy assisting and opposing flows, *Int. J. Mech. Sci.* 138 (2018) 515–523.
- [2] T. Hayat, M.I. Khan, M. Tamoor, M. Waqas, A. Alsaedi, Numerical Simulation of Heat Transfer in MHD Stagnation Point Flow of Cross Fluid Model towards a Stretched Surface, *Results In Physics* 7, 2017, pp. 1824–1827.
- [3] A. Jamaludin, R. Nazar, I. Pop, Mixed convection stagnation-point flow of Cross fluid over a shrinking sheet with suction and thermal radiation, *Phys. Stat. Mech. Appl.* 585 (2022), 126398.
- [4] A. Vaisi, K. Javaherdeh, R. Moosavi, Condensation heat transfer performance in multi-fluid compact heat exchangers with wavy and strip fins, *Int. J. Heat Mass Tran.* 182 (2022), 121968.
- [5] H. Hanif, A finite difference method to analyze heat and mass transfer in kerosene based γ -oxide nanofluid for cooling applications, *Phys. Scripta* 96 (9) (2021), 095215.
- [6] M. Saqib, H. Hanif, T. Abdeljawad, I. Khan, S. Shafie, K.S. Nisar, Heat transfer in MHD flow of maxwell fluid via fractional Cattaneo-Friedrich model: a finite difference approach, *CMC-Computers Materials & Continua* 65 (3) (2020) 1959–1973.
- [7] W. Jamshed, K.S. Nisar, R.W. Ibrahim, F. Shahzad, M.R. Eid, Thermal expansion optimization in solar aircraft using tangent hyperbolic hybrid nanofluid: a solar thermal application, *J. Mater. Res. Technol.* 14 (2021) 985–1006.
- [8] A.M. Metwally, A. Khalid, A. Khan, K. Iskakova, M. Gorji, M. Ehab, Radiation consequences on Sutterby fluid over a curved surface, *J. Eng. Thermophys.* 31 (2) (2022) 315–327.
- [9] R. Rafaqat, A. Khan, A. Zaman, F. Mabood, I. Badruddin, Magneto-hydrodynamics second grade compressible fluid flow in a wavy channel under peristalsis: application to thermal energy, *J. Energy Storage* 51 (2022), 104463.
- [10] W. Jamshed, M. Prakash, S. Devi, R.W. Ibrahim, F. Shahzad, K.S. Nisar, M.R. Eid, A. Abdel-Aty, M.M. Khashan, I.S. Yahia, A brief comparative examination of tangent hyperbolic hybrid nanofluid through a extending surface: numerical Keller–Box scheme, *Sci. Rep.* 11 (1) (2021) 1–32.
- [11] D. Lu, M.I. Afridi, U. Allauddin, U. Farooq, M. Qasim, Entropy generation in a dissipative nanofluid flow under the influence of magnetic dissipation and transpiration, *Energies* 13 (20) (2020) 5506.
- [12] M. Afridi, M. Qasim, Second law analysis of Blasius flow with nonlinear Rosseland thermal radiation in the presence of viscous dissipation, *Propulsion and Power Research* 8 (3) (2019) 234–242.
- [13] A. Bejan, *Entropy Generation Minimization: the New Thermodynamics of Finite-Size Devices and Finite-Time Processes*, CRC Press, Boca Raton, 1996.
- [14] P. Datta, P.S. Mahapatra, K. Ghosh, N.K. Manna, S. Sen, Heat transfer and entropy generation in a porous square enclosure in presence of an adiabatic block, *Transport Porous Media* 111 (2) (2015) 305–329.
- [15] I. Zahmatkesh, On the importance of thermal boundary conditions in heat transfer and entropy generation for natural convection inside a porous enclosure, *Int. J. Therm. Sci.* 47 (3) (2008) 339–346.
- [16] G.H.R. Kefayati, Simulation of natural convection and entropy generation of non-Newtonian nanofluid in a porous cavity using Buongiorno's mathematical model, *Int. J. Heat Mass Tran.* 112 (2017) 709–744.
- [17] K. Ghasemi, M. Siavashi, MHD nanofluid free convection and entropy generation in porous enclosures with different conductivity ratios, *J. Magn. Magn. Mater.* 442 (2017) 474–490.
- [18] M.H. Tilehnoee, A.S. Dogonchi, S.M. Seyyedi, A.J. Chamkha, D.D. Ganji, Magnetohydrodynamic natural convection and entropy generation analyses inside a nanofluid-filled incinerator shaped porous cavity with wavy heater block, *J. Therm. Anal. Calorimetry* 141 (5) (2020) 2033–2045.
- [19] S. Hussain, K. Mehmood, M. Sagheer, A. Farooq, Entropy generation analysis of mixed convective for in an inclined channel with cavity with Al_2O_3 -water nanofluid in porous medium, *Int. Commun. Heat Mass Tran.* 89 (2017) 198–210.
- [20] A.A. Al-Rashed, K. Kalidasan, L. Kolsi, R. Velkenedy, A. Aydi, A.K. Hussein, E.H. Malekshah, Mixed convection and entropy generation in a nanofluid filled cubical open cavity with a central isothermal block, *Int. J. Mech. Sci.* 135 (2018) 362–375.
- [21] S.S.S. Sen, M. Das, R. Mahato, S. Shaw, Entropy analysis on nonlinear radiative MHD flow of Diamond- Co_3O_4 /ethylene glycol hybrid nanofluid with catalytic effects, *Int. Commun. Heat Mass Tran.* 129 (2021), 105704.
- [22] H. Hanif, I. Khan, S. Shafie, Heat transfer exaggeration and entropy analysis in magneto-hybrid nanofluid flow over a vertical cone: a numerical study, *J. Therm. Anal. Calorimetry* 141 (5) (2020) 2001–2017.
- [23] S. Mandal, G.C. Sht, S. Shaw, O.D. Makinde, Entropy analysis of thermo-solutal stratification of nanofluid flow containing gyrotactic microorganisms over an inclined radiative stretching cylinder, *Therm. Sci. Eng. Prog.* 34 (2022), 101379.
- [24] N.N. Kumar, D.R.V.S. Sastry, S. Shaw, Irreversibility analysis of an unsteady micropolar CNT-blood nanofluid flow through a squeezing channel with activation energy-Application in drug delivery, *Comput. Methods Progr. Biomed.* 226 (2022), 107156.
- [25] H. Hanif, S. Shafie, Interaction of multi-walled carbon nanotubes in mineral oil based Maxwell nanofluid, *Sci. Rep.* 12 (1) (2022) 1–16.
- [26] H. Hanif, S. Shafie, Impact of Al_2O_3 in electrically conducting mineral oil-based maxwell nanofluid: application to the petroleum industry, *Fractal and Fractional* 6 (4) (2022) 180.
- [27] H. Hanif, S. Shafie, Application of Cattaneo heat flux to Maxwell hybrid nanofluid model: a numerical approach, *The European Physical Journal Plus* 137 (8) (2022) 1–13.
- [28] Z. Said, L.S. Sundar, A.K. Tiwari, H.M. Ali, M. Sheikholeslami, E. Bellos, H. Babar, Recent advances on the fundamental physical phenomena behind stability, dynamic motion, thermophysical properties, heat transport, applications, and challenges of nanofluids, *Phys. Rep.* 46 (2022) 1–94.
- [29] D.K. Mandal, N. Biswas, N.K. Manna, D.K. Gayen, R.S.R. Gorla, A.J. Chamkha, Thermo-fluidic transport process in a novel M-shaped cavity packed with non-Darcian porous medium and hybrid nanofluid: application of artificial neural network (ANN), *Phys. Fluids* 34 (3) (2022), 033608.
- [30] S.M. Hussain, W. Jamshed, A comparative entropy based analysis of tangent hyperbolic hybrid nanofluid flow: implementing finite difference method, *Int. Commun. Heat Mass Tran.* 129 (2021), 105671.
- [31] M.A. Qureshi, Thermal capability and entropy optimization for Prandtl-Eyring hybrid nanofluid flow in solar aircraft implementation, *Alex. Eng. J.* 61 (7) (2022) 5295–5307.
- [32] S. Parvin, S.S.P.M. Isa, W. Jamshed, R.W. Ibrahim, K.S. Nisar, Numerical treatment of 2D-Magneto double-diffusive convection flow of a Maxwell nanofluid: heat transport case study, *Case Stud. Therm. Eng.* 28 (2021), 101383.
- [33] H. Hanif, I. Khan, S. Shafie, A novel study on time-dependent viscosity model of magneto-hybrid nanofluid flow over a permeable cone: applications in material engineering, *The European Physical Journal Plus* 135 (9) (2020) 730.
- [34] H. Hanif, I. Khan, S. Shafie, A novel study on hybrid model of radiative Cu- Fe_3O_4 /water nanofluid over a cone with PHF/PWT, *Eur. Phys. J.: Spec. Top.* 230 (5) (2021) 1257–1271.
- [35] M. Afridi, M. Qasim, N.A. Khan, M. Hamdani, Heat transfer analysis of Cu- Al_2O_3 -water and Cu- Al_2O_3 -kerosene oil hybrid nanofluids in the presence of frictional heating: using 3-stage Lobatto IIIA formula, *Journal of Nanofluids* 8 (4) (2019) 885–891.
- [36] M.I. Afridi, T.A. Alkanhal, M. Qasim, I. Tlili, Entropy generation in Cu- Al_2O_3 - H_2O hybrid nanofluid flow over a curved surface with thermal dissipation, *Entropy* 21 (10) (2019) 941.
- [37] M.I. Afridi, M. Qasim, S. Saleem, Second law analysis of three dimensional dissipative flow of hybrid nanofluid, *Journal of Nanofluids* 7 (6) (2018) 1272–1280.
- [38] L. Zhang, M.M. Bhatti, E.E. Michaelides, M. Marin, R. Ellahi, Hybrid nanofluid flow towards an elastic surface with tantalum and nickel nanoparticles, under the influence of an induced magnetic field, *Eur. Phys. J.: Spec. Top.* 231 (3) (2022) 521–533.
- [39] M. Izadi, M.A. Sheremet, S.A.M. Mehryan, Natural convection of a hybrid nanofluid affected by an inclined periodic magnetic field within a porous medium, *Chin. J. Phys.* 65 (2020) 447–458.
- [40] M.R. Khan, M. Li, S. Mao, R. Ali, S. Khan, Comparative study on heat transfer and friction drag in the flow of various hybrid nanofluids effected by aligned magnetic field and nonlinear radiation, *Sci. Rep.* 11 (1) (2021) 1–14.

- [41] A. Mourad, A. Aissa, F. Mebarek-Oudina, W. Jamshed, W. Ahmed, H.M. Ali, A.M. Rashad, Galerkin finite element analysis of thermal aspects of Fe₃O₄-MWCNT/water hybrid nanofluid filled in wavy enclosure with uniform magnetic field effect, *Int. Commun. Heat Mass Tran.* 126 (2021), 105461.
- [42] H.T. Rostami, M.F. Najafabadi, Kh Hosseinzadeh, D.D. Ganji, Investigation of mixture-based dusty hybrid nanofluid flow in porous media affected by magnetic field using RBF method, *Int. J. Ambient Energy* 43 (1) (2022) 6425–6435.
- [43] M.M. Rashidi, M. Sadri, M.A. Sheremet, Numerical simulation of hybrid nanofluid mixed convection in a lid-driven square cavity with magnetic field using high-order compact scheme, *Nanomaterials* 11 (9) (2021) 2250.
- [44] N. Biswas, M.K. Mondal, D.K. Mandal, N.K. Manna, R.S.R. Gorla, A.J. Chamkha, A narrative loom of hybrid nanofluid-filled wavy walled tilted porous enclosure imposing a partially active magnetic field, *Int. J. Mech. Sci.* 217 (2022), 107028. ±.
- [45] A. Aanam, P.G. Siddheshwar, S.S. Nagouda, S. Pranesh, Effects of variable viscosity and rotation modulation on ferroconvection, *J. Therm. Anal. Calorimetry* 147 (7) (2022) 4667–4682.
- [46] A.S. Idowu, M.T. Akolade, J.U. Abubakar, B.O. Falodun, MHD free convective heat and mass transfer flow of dissipative Casson fluid with variable viscosity and thermal conductivity effects, *J. Taibah Univ. Sci.* 14 (1) (2020) 851–862.
- [47] Y. Akbar, F.M. Abbasi, Impact of variable viscosity on peristaltic motion with entropy generation, *Int. Commun. Heat Mass Tran.* 118 (2020), 104826.
- [48] A.U. Jan, E.R. El-Zahar, N.A. Shah, R. Shah, Computation of magnetized Couette–Poiseuille thermal flow of couple stress between two analogous plate with variable viscosity suspending the hafnium particles, *Int. Commun. Heat Mass Tran.* 134 (2022), 106042.
- [49] F. Ismail, M. Qayyum, I. Ullah, S.I.A. Shah, M.M. Alam, A. Aziz, Fractional Analysis of Thin-Film Flow in the Presence of Thermal Conductivity and Variable Viscosity, *Waves in Random and Complex Media*, 2022, pp. 1–19.
- [50] H.J. Xu, Z.B. Xing, F.Q. Wang, Z.M. Cheng, Review on Heat Conduction, Heat Convection, Thermal Radiation and Phase Change Heat Transfer of Nanofluids in Porous Media: Fundamentals and Applications, *Chemical Engineering Science* 195, 2019, pp. 462–483.
- [51] A. Wakif, A. Chamkha, T. Thumma, I.L. Animesaun, R. Sehaqui, Thermal radiation and surface roughness effects on the thermo-magneto-hydrodynamic stability of alumina–copper oxide hybrid nanofluids utilizing the generalized Buongiorno’s nanofluid model, *J. Therm. Anal. Calorimetry* 143 (2) (2021) 1201–1220.
- [52] J. Chen, C.Y. Zhao, B.X. Wang, Effect of nanoparticle aggregation on the thermal radiation properties of nanofluids: an experimental and theoretical study, *Int. J. Heat Mass Tran.* 154 (2020), 119690.
- [53] P. Agrawal, P.K. Dadheech, R.N. Jat, K.S. Nisar, M. Bohra, S.D. Purohit, Magneto Marangoni flow of γ -Al₂O₃ nanofluids with thermal radiation and heat source/sink effects over a stretching surface embedded in porous medium, *Case Stud. Therm. Eng.* 23 (2021), 100802.
- [54] J. Prakash, E.P. Siva, D. Tripathi, S. Kuharat, O.A. Bég, Peristaltic Pumping of Magnetic Nanofluids with Thermal Radiation and Temperature-dependent Viscosity Effects: Modelling a Solar Magneto-Biomimetic Nanopump, *Renewable Energy* 133, 2019, pp. 1308–1326.
- [55] S.A. Khan, B. Ali, C. Eze, K.T. Lau, L. Ali, J. Chen, J. Zhao, Magnetic dipole and thermal radiation impacts on stagnation point flow of micropolar based nanofluids over a vertically stretching sheet: finite element approach, *Processes* 9 (7) (2021) 1089.
- [56] L. Ali, B. Ali, X. Liu, T. Iqbal, R.M. Zulqarnain, M. Javid, A comparative study of unsteady MHD Falkner–Skan wedge flow for non-Newtonian nanofluids considering thermal radiation and activation energy, *Chin. J. Phys.* 77 (2022) 1625–1638.
- [57] S. Shaw, S.S. Samantary, A. Misra, M.K. Nayak, O.D. Makinde, Hydromagnetic flow and thermal interpretations of Cross hybrid nanofluid influenced by linear, nonlinear and quadratic thermal radiations for any Prandtl number, *Int. Commun. Heat Mass Tran.* 130 (2022), 105816.
- [58] T. Zubair, M. Usman, K.S. Nisar, I. Khan, M. Ghamkhar, M. Ahmad, Crank–Nicolson scheme to examine the fractional-order unsteady nanofluid flow of free convection of viscous fluids, *PLoS One* 17 (3) (2022), e0261860.
- [59] S.B. Goud, W. Jamshed, R. Safdar, Y.D. Reddy, M.M. Alanazi, H.Y. Zahran, M.R. Eid, Chemical reactive and viscous dissipative flow of magneto nanofluid via natural convection by employing Galerkin finite element technique, *Coatings* 12 (2) (2022) 151.
- [60] H. Hanif, Cattaneo–Friedrich and Crank–Nicolson analysis of upper-convected Maxwell fluid along a vertical plate, *Chaos, Solit. Fractals* 153 (2021), 111463.
- [61] H. Hanif, A computational approach for boundary layer flow and heat transfer of fractional Maxwell fluid, *Math. Comput. Simulat.* 191 (2022) 1–13.
- [62] F.A. Soomro, R. Ul Haq, M. Hamid, Brownian motion and thermophoretic effects on non-Newtonian nanofluid flow via Crank–Nicolson scheme, *Arch. Appl. Mech.* 91 (7) (2021) 3303–3313.
- [63] E.M. Salilih, N.H. Abu-Hamdeh, A. Khoshaim, A. Karimipour, Numerical Crank–Nicolson transient thermal analysis of a single U-tube vertical ground battery borehole heat exchanger filled with the phase change material, *J. Energy Storage* 53 (2022), 105119.
- [64] A.A. Khan, F. Zaib, A. Zaman, Effects of entropy generation on Powell Eyring fluid in a porous channel, *J. Braz. Soc. Mech. Sci. Eng.* 39 (12) (2017) 5027–5036.
- [65] T. Hayat, S. Farooq, A. Alsaedi, Mixed convection peristaltic motion of copper-water nanomaterial with velocity slip effects in a curved channel, *Comput. Methods Progr. Biomed.* 142 (2017) 117–128.
- [66] S. Farooq, A. Alsaedi, T. Hayat, B. Ahmad, Peristaltic transport of Johnson–Segalman fluid with homogeneous-heterogeneous reactions: a numerical analysis, *J. Braz. Soc. Mech. Sci. Eng.* 40 (2018) 242.
- [67] S. Farooq, T. Hayat, A. Alsaedi, S. Asghar, Mixed convection peristalsis of carbon nanotubes with thermal radiation and entropy generation, *J. Mol. Liq.* 250 (2018) 451–467.
- [68] M.I. Khan, T.S. Farooq, T. Hayat, F. Shah, A. Alsaedi, Numerical simulation for entropy generation in peristaltic flow with single and multi-wall carbon nanotubes, *Int. J. Numer. Methods Heat Fluid Flow* 29 (12) (2019) 4684–4705.
- [69] S. Farooq, T. Hayat, M. Ijaz Khan, A. Alsaedi, Entropy generation minimization (EGM) in magneto peristalsis with variable properties, *Comput. Methods Progr. Biomed.* 186 (2020), 105045.
- [70] S.Z. Abbas, S. Farooq, Y.M. Chu, W. Chammmam, W.A. Khan, A. Riahi, H.A. Rebei, M. Zaway, Numerical study of nanofluid transport subjected to the collective approach of generalized slip condition and radiative phenomenon, *Arabian J. Sci. Eng.* 46 (2021) 6049–6059.
- [71] M.I. Khan, S. Qayyum, S. Farooq, M.Y. Chu, S. Kadry, Modeling and simulation of micro-rotation and spin gradient viscosity for ferromagnetic hybrid (Manganese Zinc Ferrite, Nickel Zinc Ferrite) nanofluids, *Math. Comput. Simulat.* 185 (2021) 497–509.
- [72] F. Bibi, T. Hayat, S. Farooq, A.A. Khan, A. Alsaedi, Entropy generation analysis in peristaltic motion of Sisko material with variable viscosity and thermal conductivity, *J. Therm. Anal. Calorimetry* 143 (2021) 363–375.